PERGAMON

International Journal of Heat and Mass Transfer 43 (2000) 2807–2819

International Journal of HEAT and MASS TRANSFER

www.elsevier.com/locate/ijhmt

Measuring interfacial waves on film flowing down a vertical plate wall in the entry region using laser focus displacement meters

Tomoji Takamasa[a,*], Tatsuya Hazuku[b]

[a]*Department of Marine Engineering, Tokyo University of Mercantile Marine Etchujima, Koto-ku, Tokyo 135-8533 Japan*
[b]*Babcock-Hitachi K. K., Hamamatsu-cho, Minato-ku, Tokyo 105-6107, Japan*

Abstract

Waves on a film flowing down a vertical wall appear in many processes. The resulting interfacial waves show fascinating nonlinear phenomena, including solitary waves and complex disordered patterns. Measurements have often been made of these phenomena using electrical resistance or electrical capacitance methods, optical methods, and laser beam methods. This paper presents a new way of measuring the interfacial waves on a film flowing down a vertical plate wall in an entry region, using two laser focus displacement meters. The purpose of the study was to clarify the effectiveness of the new method for obtaining detailed information on the waves, and to investigate the effect of the entry length on the phenomena. With this method, accurate measurements of film thickness were achieved in real time with a sensitivity of 2 μm and 1 kHz. The error caused by refraction of the laser beam passing through a transparent wall was clarified. The present results for wave velocity and maximum film thickness agreed well with past experimental and theoretical studies. In short entry length conditions, the average measured film thickness and wave velocity agreed with those calculated using Nusselt's Law, indicating that the flow is laminar even at a high flow rate. As a result of this study, an empirical equation expressing wave frequency in the entry region was formulated.

Keywords: Flow measurement; Local measurement; Laser-aided diagnostics; Free surface flow; Film; Refraction; Wave; Velocity; Frequency; Plate; Wall; Vertical flow; Multiphase flow

1. Introduction

Waves on a film flowing down a vertical wall are encountered in many applications, such as heat exchangers, condensers, and chemical-process equipments. Complex interactions between the liquid-turbulence structure in the film and gas–liquid interfaces govern the physical properties of such flows. The resulting interfacial waves show fascinating nonlinear phenomena, including solitary waves and complex disordered patterns. To elucidate these phenomena in detail, spatial-temporal knowledge of the interfacial waves is essential. Pertinent details include the minimum and maximum film thickness, or wave heights, the average film thickness, and the velocity and frequency of the waves.

* Corresponding author. Tel.: +81-3-5245-7406; fax: +81-3-5245-7336.
E-mail address: takamasa@ipc.tosho-u.ac.jp (T. Takamasa).

0017-9310/00/$ - see front matter
PII: S0017-9310(99)00335-X

Nomenclature

A	wave amplitude
C_W	wave velocity
d	distance between laser head and window
f_W	wave frequency
g	acceleration of gravity
h	wave height
$\bar{h}$	average wave height
K_F	physical properties group ($\rho^3\nu^4 g/\sigma^3$)
L	entry length
N	refractive index
N_{Cw}	dimensionless wave velocity ($C_W/(\nu g)^{1/3}$)
N_{f_W}	dimensionless wave frequency ($f_W(\nu/g^2)^{1/3}$)
N_L	dimensionless entry length ($L(g/\nu^2)^{1/3}$)
Re	Reynolds number
$N_{\delta_{max}}$	dimensionless maximum film thickness ($\delta_{max}(g/\nu^2)^{1/3}$)
N_λ	dimensionless wave separation ($\lambda(g/\nu^2)^{1/3}$)
t	time
U_0	average liquid velocity $\Gamma/\bar{\delta}$)
Z	distance between the beam spots

Greek symbols

α	dimensionless wave velocity defined by average liquid velocity (C_W/U_0)
Γ	volumetric flow rate per unit wetted perimeter
δ	liquid film thickness
$\bar{\delta}$	average film thickness
κ	angle of the incidence
λ	wave separation
ν	kinematic viscosity
ρ	density of liquid
σ	surface tension
ω	phase delay

Subscripts

A, F, W	air, fluid, wall
r, m	real, measured
max, min	maximum, minimum

Many measurements have been made of these phenomena, using electrical-resistance or electrical-capacitance methods and other methods [1–5]. In the electrical methods, the film thickness is calculated from the resistance or capacitance between the sensors. The instantaneous film thickness, or crest and roughness of the wave, cannot be measured by this method, but the spatial average film thickness can be determined. On the other hand, some researchers have used a laser displacement sensor [6] and a supersonic echo method [7] to measure the wave on a film. The laser displacement sensor, comprising a semiconductor laser and a position-sensitive detector, detects the target position using a triangular relationship. The laser beam reflected from the target is focused on the position-sensitive detector, forming a beam spot. The laser displacement sensor and the supersonic echo method have an advantage over the electrical method: these techniques involve high spatial resolution, and they do not disturb the flow. The techniques do, however, present one problem: if the curvature of the interfacial wave is large, the reflected beam and the sonic wave cannot reach the detector. A small wave or a wave that has a large curvature on its interface cannot be measured accurately by these techniques. Recently, a new laser focus displacement meter (LFD, Keyence Co. Japan, Model LT 8100) was developed to detect scratches on the ICs or other electronic devices. This sensor has the potential to solve the curvature problem and to measure waves on a film at high spatial and temporal resolutions.

This paper presents a measurement of the interfacial waves on a film flowing down a vertical plate wall, using a pair of LFDs. The purpose of the study was to develop a wave measurement method using LFDs that allow accurate measurements of film thickness in real time with a sensitivity of 2 μm and 1 kHz, and to investigate the waves on a falling film in an entry region. Although considerable efforts were made in the past to study the phenomena of falling film in a fully developed region, 1–2 m below the inlet section, very few detailed measurements have been made of phenomena in the entry region, which is considered more important for industrial design than the fully developed region. One reason why wave measurements had not been made in the entry region might be that in the past we had no accurate measurement technique for thin films.

2. Principle of measurements

2.1. Principle of LFD

Fig. 1 shows a schematic diagram of an LFD. The conical laser beam emitted from a semiconductor laser passes through a half-reflection mirror and an objective lens, and then reaches the target surface. The scat-

tering light reflected from the target passes backward through the objective lens, is reflected by the half-reflection mirror, and reaches a pinhole. The objective lens is moved frequently by a diapason, or a tuning fork. The displacement of the diapason, which moves coincidentally with the lens, is detected by a position-sensitive detector. The reflection beam appears on a light-sensitive element at the rear of the pinhole when the laser beam is focused on the target, as explained by mutual-focusing theory. The displacement of the target from the LFD can then be determined by detecting the displacement of the object lens when the signal from the sensing element is on. This principle makes possible accurate measurement of the wave height or film thickness, even if the wave surface has a large curvature. The sensor has a measurement range of 28 ± 1 mm from the laser head. The diameter of the beam spot on the target is 2 μm, and the spatial resolution is 0.2 μm. The temporal resolution, which depends on the frequency of the tuning fork, was 1.4 kHz for the original LFD. To reduce measurement error in the system, the output signal from the LFD is the average of two measurements. The temporal resolution of the present LFD system thus is 0.7 kHz. The principle behind an LFD measuring the distance between the sensor and the target is the same as that of a camera focusing on a target by a motor-driven objective lens in daylight. In the LFD system, high temporal and spatial resolutions are realized by using a tuning fork and a laser beam. As a result, the tiniest roughness of a wave can be detected.

2.2. Calibration for refraction

We can measure liquid film thickness using an LFD from the film-surface side (front measurement) or from the back of a transparent plate (back measurement). In the back-measuring LFD, it is necessary to estimate the displacement error caused by refraction of the laser beam passing the plate or the window surfaces on both sides.

First, the displacement error is examined theoretically by the law of refraction. The LFD can measure the liquid and the plate surfaces in one movement cycle of the objective lens, and film thickness δ can be calculated from the displacement difference between the two signals, as shown in Fig. 2. The real film thickness, calculated from the measured displacement of the film thicknessm δ_m, is denoted as follows:

$$\delta = \delta_m \frac{\tan \kappa_A}{\tan \kappa_F} \tag{1}$$

where κ is the angle of incidence at the surface, and subscripts A and F represent air and fluid, respectively. From Snell's law:

$$N_A \sin \kappa_A = N_F \sin \kappa_F \tag{2}$$

where N is the refractive index. From Eq. (2), the angle of incidence at the window–fluid interface, κ_F, can be obtained as follows:

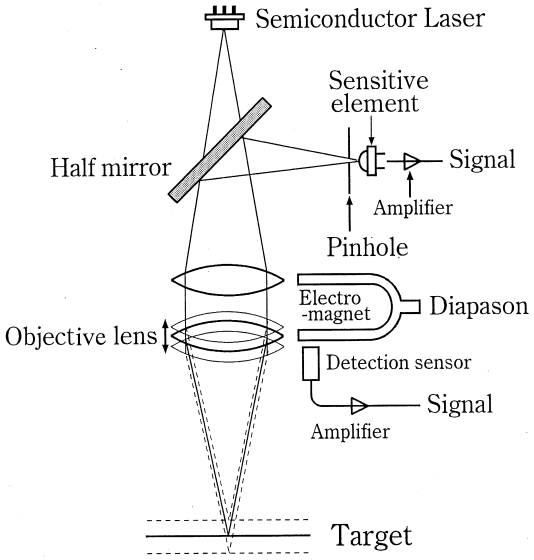

Fig. 1. Laser focus displacement meter.

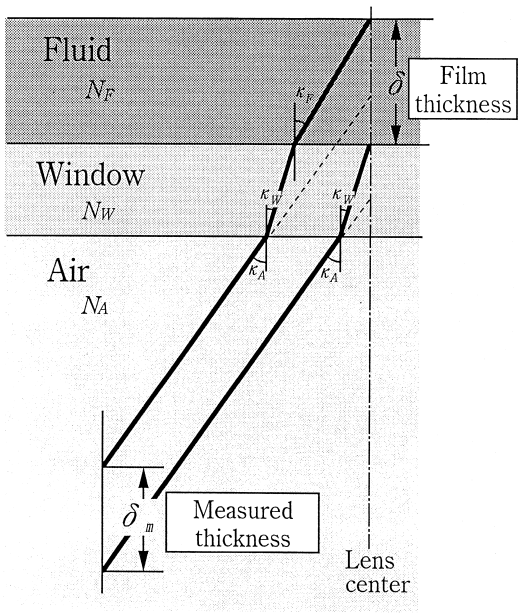

Fig. 2. Laser beam path.

$$\kappa_F = \sin^{-1}\left[\frac{N_A}{N_F}(\sin \kappa_A)\right] \quad (3)$$

Substituting in the refractive indexes of air and water, $N_A = 1$ and $N_W = 1.32$, and the angle of incidence of a laser beam from the LFD to the target, $\kappa_A = 11.5°$, the real film thickness δ can be calculated from Eqs. (1) and (3).

$$\delta = 1.332\delta_m \quad (4)$$

This simple equation shows that the real film thickness is independent of the thickness and refractive index of the window, and of the distance between the laser head and the window, when the film thickness is calculated from the displacement between the two signals for the fluid and window surfaces.

Second, the displacement error was examined experimentally through the following two preliminary tests. Fig. 3 illustrates the apparatus used in the first preliminary test, which consists of a test cylinder and a water tank with a window at the bottom. The cylinder can be traversed vertically 1 μm by one signal pulse transmitted from a personal computer. Distance δ_r between the surfaces of the cylinder bottom and the window, which is equivalent to a film thickness, was detected by an LFD installed under the window. To check the effect of the distance between the LFD head and the window surface d on measured distance δ_m between the surfaces of the cylinder bottom and the window, a micrometer can traverse the LFD vertically. Fig. 4 shows the relationship between δ_r and δ_m. Marks representing different distances between the LFD head and window surface d overlap in the figure, which means that the distance little affects the measured distance δ_m. The solid circles represent the corrected δ_m calculated from Eq. (4). The corrected δ_m agrees with the real distance δ_r with in a 1.5% margin of error, which is represented by a straight line in the figure.

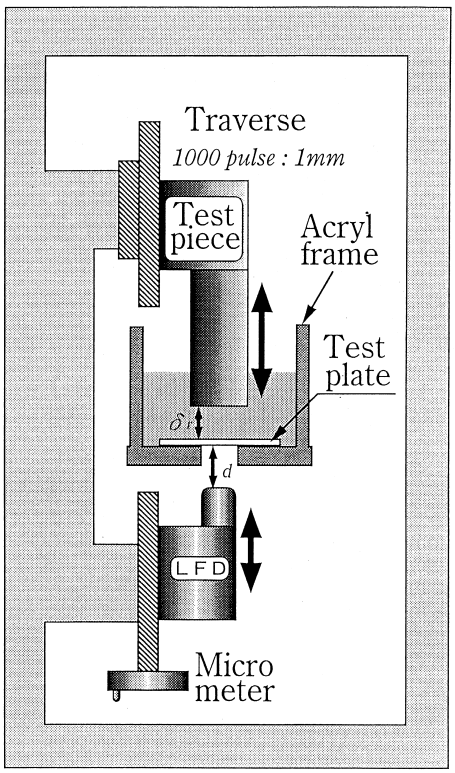

Fig. 3. Apparatus for the preliminary test.

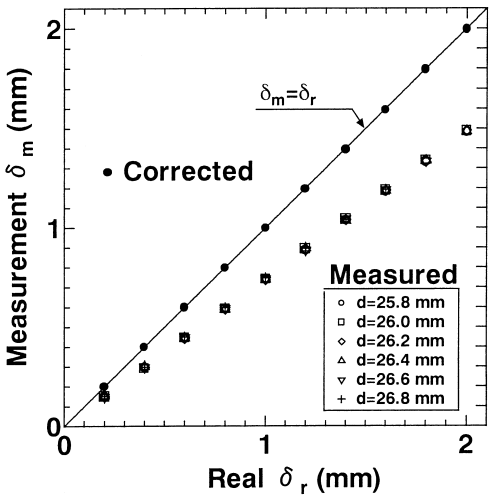

Fig. 4. Refraction error and corrected film thickness.

In the second preliminary test, the instantaneous film thickness was measured by front- and back-measuring LFDs. The beam spots were placed 1.5 mm apart, so that the two beams would not interfere with each other. Fig. 5 shows typical results of instantaneous film thickness measurements by front- and back-measuring LFDs. The corrected film thickness,

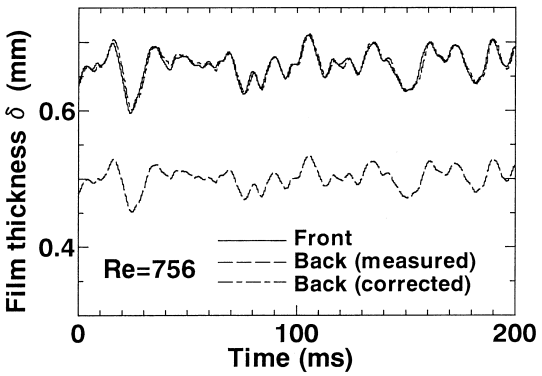

Fig. 5. Measured and corrected interfacial wave data.

which is calculated by Eq. (4) and represented by a dot-dash line in the figure, agrees well with the front measurement thickness represented by a solid line. The results of the two preliminary tests confirmed that Eq. (4) could be used to estimate the displacement error caused by refraction of the laser beam at the window surfaces and that film thickness could be measured accurately using an LFD positioned at the window side.

We found some erroneous front measurement film thickness at a low liquid flow rate or under thin film conditions, as shown in Fig. 6. In front measurement, some waves are missed, as indicated by the circles in the figure. When a thin-film wave has a large curvature, an erroneous signal for window surface displacement, caused by the refracted beam passing through the wave surface, interferes with the signal for the wave surface, and hence the film thickness cannot be detected. In the present experiments, erroneous front measurement were found when $\delta < 0.6$ mm. Using a back-measuring LFD is therefore recommended to measure such thin film thickness accurately.

2.3. Measurement of wave velocity

The wave velocity was measured using the front- and back-measuring LFDs, as shown in Fig. 7. Time delay t between the LFDs is denoted by wave frequency f_W and phase angle ω:

$$t = \frac{\omega}{2\pi f_W} \tag{5}$$

Wave velocity C_W is calculated by Eq. (6):

$$C_W = \frac{2\pi f_W}{\omega} Z \tag{6}$$

where Z is the distance between the beam spots. In the present experiments, the distance was set at 2.5 mm through this study. Waves on a film consist of many frequency components. Assuming that the wave velocity is independent of the frequency component, a straight line can be drawn that represents the relationship between frequency f_W and phase-lag angle ω. The slope of the line becomes steeper as the wave velocity increases. When a wave propagates in one direction, it is possible to calculate the wave velocity if phase phase-lag ω is smaller than one cycle of the wave or $\omega < 2\pi$. By substituting in this condition, the relationship among the measurable wave velocity and distance between the beam spots as well as wave frequency is obtained from Eq. (6).

$$C_W > f_W Z \tag{7}$$

Four or more samples in one cycle of a wave are

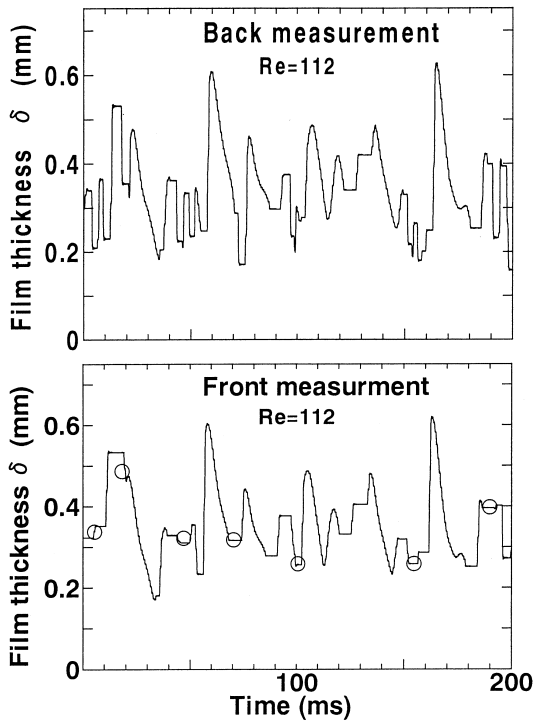

Fig. 6. Wave phenomena on thin-liquid film.

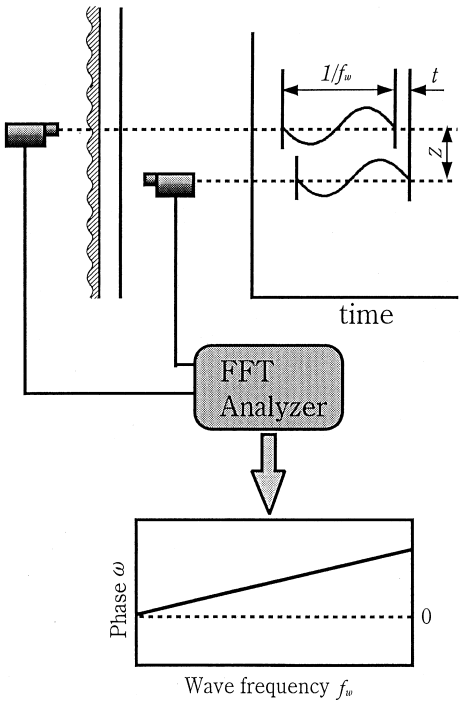

Fig. 7. Method for measuring interfacial wave velocity.

necessary to identify the wave. Because the sampling frequency f_S in LFD measurements is 0.7 kHz, the frequency of a measurable wave f_t is:

$$f_t < \frac{1}{4} f_S = 175 \tag{8}$$

Fig. 8 illustrates the measurement limitation in the present system as a function of the frequency and distance between the beam spots, calculated from Eqs. (7) and (8). It is reasonable to measure the wave velocity using a pair of LFDs positioned at the same side for data processing. The LFD thickness, however, is the distance between the beam spots, which is larger than 33 mm, when the LFDs are positioned at the same side. Such a large distance significantly reduces measurement area as shown in the figure. Wave velocity was therefore measured using front- and back-measuring LFDs in the present experiments. The signal provided from the back-measuring LFD was corrected by Eq. (4).

3. Apparatus

Fig. 9 shows the apparatus used in the present experiments. Water was pumped into a head water tank from a feed water tank, passing through a pure-water generator that purified tap water to an electrical conductivity of less than 1 μS/cm. The level of the head water tank was kept constant by an overflow outlet. The water temperature was maintained at a level of 15 $\pm$ 0.5°C by a submerged heater and a cooler in the feed water tank. After flowing down through flow-control valves, a horizontal Teflon tube, and a test section, the water was drained from the system. The length and width of the test section were 460 and 210 mm, respectively. A uniformly flowing liquid film was achieved by use of a Teflon tube with many 1 mm holes in the wall and a slit positioned above the test section. The uniformity was confirmed by LFD measurements which located at three points in width of the test section, the center and points 100 mm apart from the center, respectively. The discrepancies among them were less than 5% in minimum, maximum and average film thickness as well as wave velocity. Two thermocouples in the water tank and drain tube measured the water temperature. The liquid flow rate was measured by a volume flowmeter installed at the drain tube. The film thickness was measured using the LFD positioned at $L = 133.5$, 166.5, 233.5, 266.5, 333.5, and 366.5 mm down from the film entrance. The signal provided from the LFDs was transmitted into a personal computer with a sampling frequency of 1 kHz. The experiments were performed with Reynolds number (Re) ranging from 32 to 706, calculated from a volumetric flow rate and wetted perimeter. Table 1 shows the settings used in the experiments.

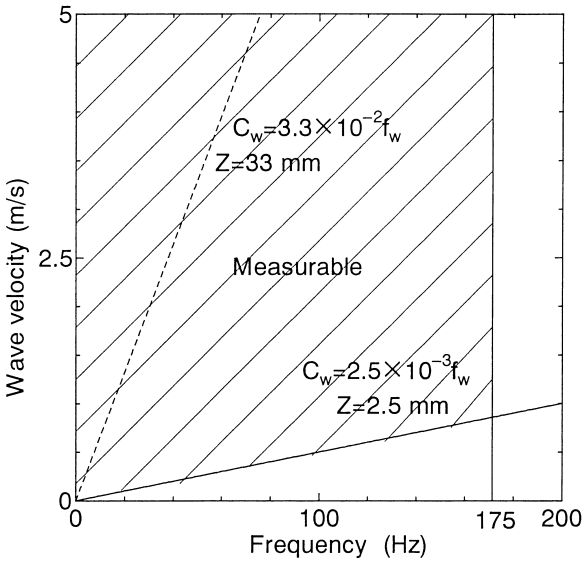

Fig. 8. Measurable frequency and wave velocity.

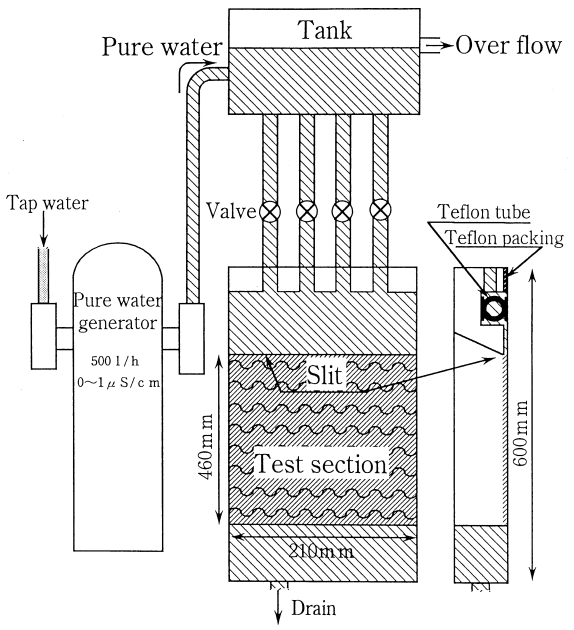

Fig. 9. Apparatus for the experiment on film flowing down a vertical wall.

Table 1
Experimental settings

Position	*Re*	Mean temperature
Film thickness		
L = 133.5 mm, 1066.5 mm	56, 101, 269, 344, 373, 439, 531, 557, 606, 631, 649, 704	
L = 233.5 mm, 266.5 mm	79, 147, 254, 345, 373, 422, 530, 549, 593, 639, 649, 706	15.0 ± 0.5°C
L = 333.5 mm, 366.5 mm	78, 135, 218, 344, 366, 431, 527, 561, 606, 639, 649, 702	
Wave velocity		
L = 250 mm	32, 96, 135, 178, 255, 339, 519, 629, 676	15.0 ± 0.5 °C

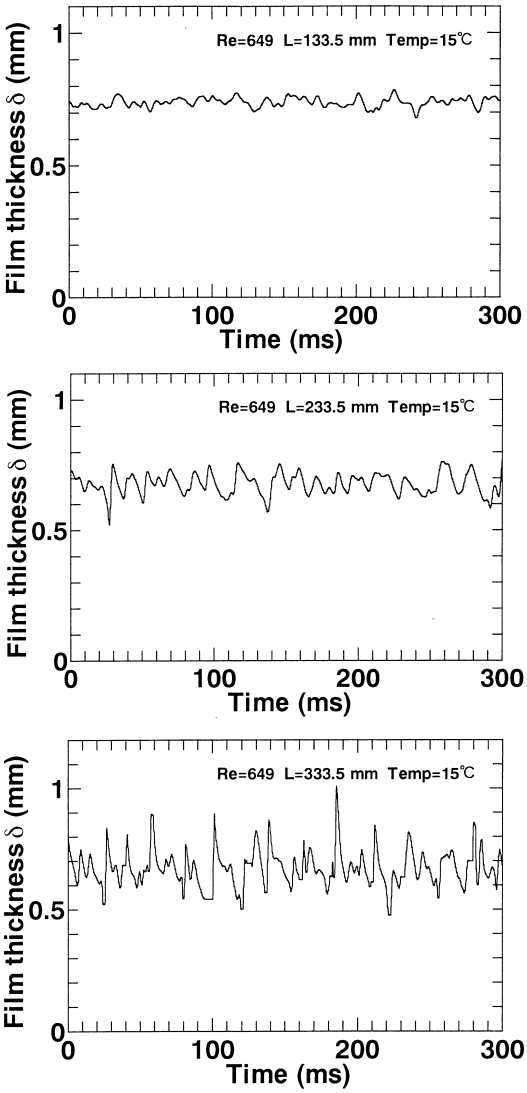

Fig. 10. Effect of entry length on interfacial waves.

4. Results

4.1. Waves on falling film

Fig. 10 shows the effect of entry length on the interfacial waves on a falling film. As shown in the figure, ripples smaller than 0.1 mm are generated on the wave in conditions of high Reynolds number and short entry length. To the naked eye, the surface of the film in that condition seemed flat as a mirror. No method other than the LFD system can accurately measure ripples or such fine waves. As the entry length increases, the ripple grows to a solitary wave about 0.5 mm in height. At the entry length of $L = 333.5$ mm, the wave becomes a two-wave system, as observed by Takahama et al. [8] in a fully developed region. Ripples and solitary waves are formulated coincidentally in two-wave system. The effect of entry length on the

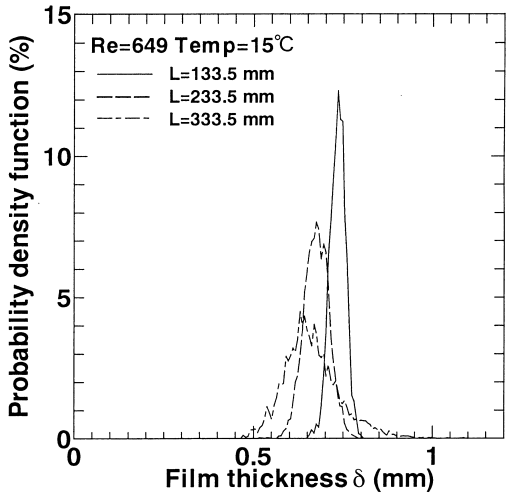

Fig. 11. Effect of entry length on probability density function of film thickness.

distribution of probability density function in film thickness is shown in Fig. 11. The distribution is symmetrical and has a sharp peak at the short entry length condition with $L = 133.5$ mm. As the entry length increases, the distribution becomes asymmetrical and the sharpness of the peak diminishes. These facts indicate that the accelerated flow reduces the film thickness, the wave grows larger and becomes a two-wave system, as the entry length increases.

Fig. 12 shows the effect of liquid flow rate on the interfacial waves. A two-wave system is generated in the low flow rate condition with $Re = 79$, which consists of solitary waves of 0.6 mm in amplitude generated at the same frequency and ripples between the solitary waves. As flow rate increases, the wave frequency increases and the amplitude decreases. Solitary waves diminish, and the waves become disordered ripples of 0.2 mm in amplitude when $Re = 706$. The effect of flow rate on the probability density function of film thickness is shown in Fig. 13. Distribution of the function spreads over wide range of film thickness in the low flow rate condition with $Re = 79$, indicating a large wave amplitude. The distributions are symmetrical and have almost identical sharp peaks with consistent width and height when $Re > 300$, indicating a wave amplitude that is small and independent of flow rate. This fact that the wave amplitude decreases as flow rate increases in the entry region is contrary to the results obtained in the past [8] in a fully developed region. The reason for this is that time required to reach the measurement position is a key factor in the

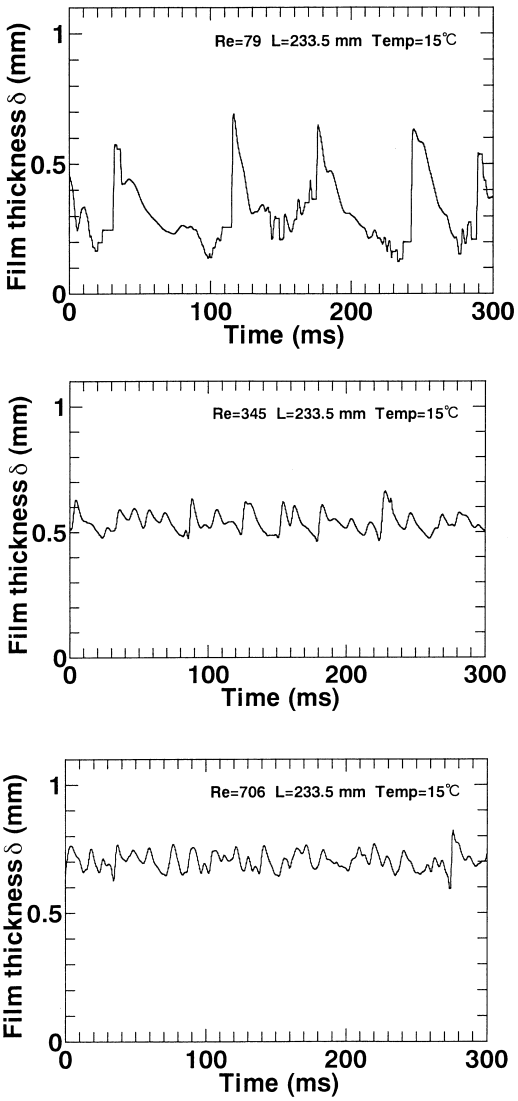

Fig. 12. Effect of flow rate on interfacial waves.

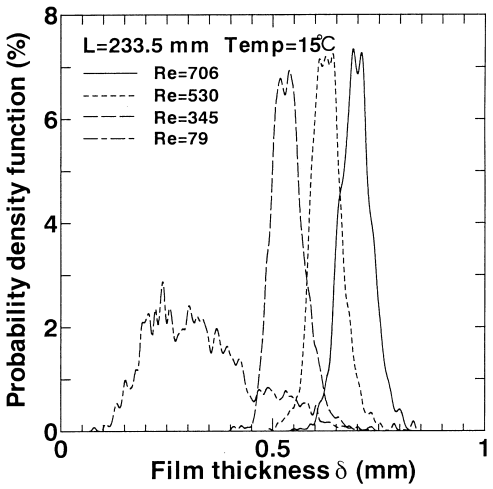

Fig. 13. Effect of flow rate on probability density function of film thickness.

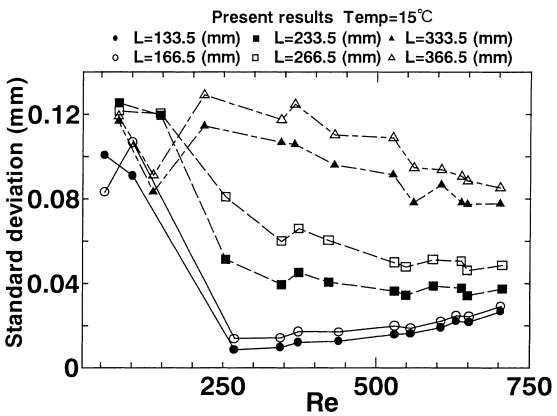

Fig. 14. Standard deviation.

growth of the wave. As the flow rate or the Reynolds number increases, the velocity of the flow increases, which shortens the time required to reach the measuring position from the film entrance. The wave thus cannot grow sufficiently if there is a high flow rate or the high Reynolds number. On the other hand, there is enough time for the waves to coalesce and grow into a solitary wave in low flow rates.

The standard deviations of the film thickness, as affected by entry length and flow rate, are shown in Fig. 14. In low Reynolds number conditions, with $Re < 250$, the standard deviation or roughness of the wave is independent of the entry length. On the other hand, the standard deviation is affected significantly by entry length in conditions of high Reynolds number, at $Re > 250$. Standard deviations increase and the waves grow as the entry length increases. Mori et al. measured falling film down tube's inner wall using electrical probes [9]. The results obtained by Mori showed that the standard deviations were independent of the entry length when Re was below the 200–350 range and increased with entry length when Re was above the 200–350 range, in a manner similar to that of the present experiments.

Efforts have been made to clarify the mechanism behind falling film in by studying the average film thickness. In the present study, the average film thickness was calculated from arithmetic average of the samples measured by the LFD positioned at window side.

$$\bar{\delta} = \frac{1}{n}\sum_{i=1}^{n}\delta_i \tag{9}$$

Fig. 15 shows the relationship between average film thickness and the Reynolds number as well as the entry length. The solid line in the figure represents a theoretical Eq. (10) for laminar flow conditions, calculated from Nusselt's Law [10].

$$\bar{\delta} = \left(\frac{3\nu^2 Re}{g}\right)^{1/3} \tag{10}$$

Theoretical Eq. (11), for turbulent flow conditions, calculated from Karman's velocity profile, is plotted in the figure as a universal velocity profile [4].

$$\left(3.0 + 2.5\ln\bar{\delta}^{+}\right)\bar{\delta}^{+} = Re + 64 \tag{11}$$

$$\bar{\delta}^{+} = u^{*}\frac{\bar{\delta}}{\nu} \tag{12}$$

Friction velocity u^* is calculated from the balance between the wall friction and gravitational force.

$$u^{*} = \sqrt{g\bar{\delta}} \tag{13}$$

The broken lines represent empirical equations obtained by Brauer (14) [11], Takahama (15) [8], and Aragaki (16) [12], respectively. Aragaki's is a modification of Henstock and Hanratty's equation [13] using a correlation factor for the wavy surface.

$$\bar{\delta} = 0.302\left(\frac{3\nu^2}{g}\right)^{1/3} Re^{0.526} \tag{14}$$

$$\bar{\delta} = 0.473\left(\frac{\nu^2}{g}\right)^{1/3} Re^{0.526} \tag{15}$$

$$\bar{\delta} = \left(\frac{\nu^2}{g}\right)^{1/3}\left[8.92Re^{5/2} + 4.04\times10^{-5}Re^{9/2}\right]^{2/15} \tag{16}$$

The present data agree with Nusselt's theoretical equation in the short entry region, thus indicating the

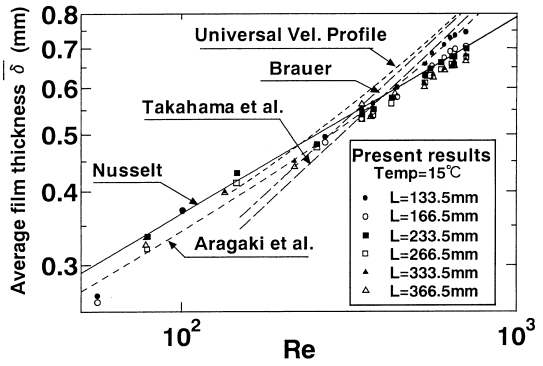

Fig. 15. Average film thickness.

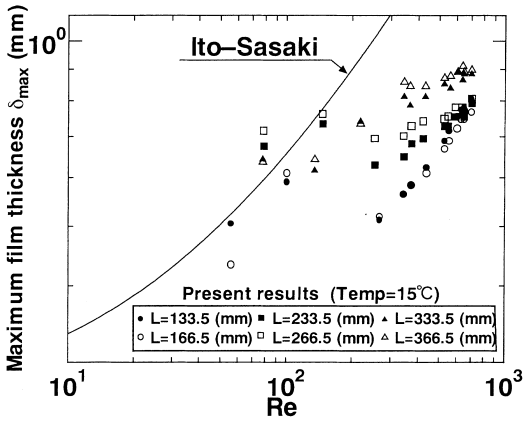

Fig. 16. Maximum film thickness.

flow to be laminar even at a high flow rate. The average film thickness is independent of the entry length when $Re < 250$. On the other hand, the average film thickness tends to decrease as the entry length increases when $Re > 250$, indicating the flow is underdeveloped.

Fig. 16 through Fig. 18 show the results of calculating maximum film thickness δ_{max}, minimum film thickness δ_{min} and average wave height $\bar{h}$. The minimum and maximum film thickness were calculated with a 99% and 1% probability of film existence, respectively [14]. The arithmetically averaged distance, h, between the minimum film thickness and crest of each wave was defined as the average wave height $\bar{h}$. Many empirical equations exist for calculating the minimum and maximum film thickness and average wave height of a film flowing down a vertical wall. In the figures, the solid lines are obtained by Ito–Sasaki's empirical equations for a film flowing down the outer surface of a vertical tube [15].

$$h_{max} = 1.78 \times 10^{-5} Re^{0.68} \tag{17}$$

$$\delta_{min} = 4.54\left(\frac{g}{\nu^2}\right)^{-1/3} \tag{18}$$

$$\delta_{max} = h_{max} + \delta_{min} \tag{19}$$

$$\bar{h} = 2.12 \times 10^{-5} Re^{0.53} \tag{20}$$

where g is the acceleration of gravity and ν is the kinematic viscosity of the fluid. Ito and Sasaki used a needle contact technique to measure the film thickness at 1600 mm from the film entrance.

As shown in Fig. 16, the present data of the maximum film thickness δ_{max} are affected little by the entry length, and agree with those calculated by Ito–Sasaki's equation, at low Reynolds numbers, $Re < 250$. On the other hand, δ_{max} increases with entry length when $Re > 250$. Minimum film thickness δ_{min} is independent of the entry length in a manner similar to that of δ_{max}, at low Reynolds numbers, $Re < 250$, as shown in Fig. 17. At high Reynolds numbers, δ_{min} increases as entry length decreases, and it tends to agree with Ito–Sasaki's equation. The entry length affects average wave height $\bar{h}$ when $Re > 250$ as shown in Fig. 18, in approximately the same way as the results of the standard deviations and δ_{max}, as well as δ_{min}. The present data for $\bar{h}$ in the long entry condition, with $L = 366.5$ mm, agree well with those calculated by Ito–Sasaki's equation.

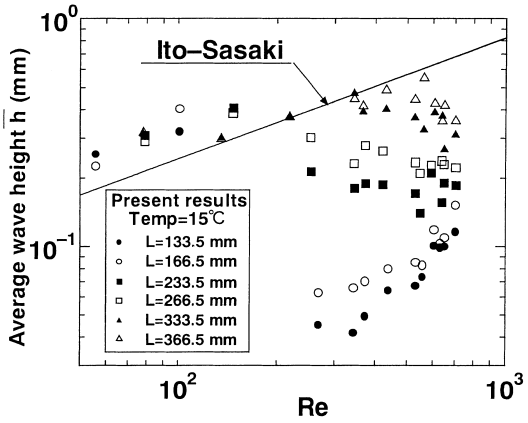

Fig. 18. Average wave height.

4.2. Velocity and separation of waves

As described in the introduction, the wave velocity was measured using the front-and back-measuring

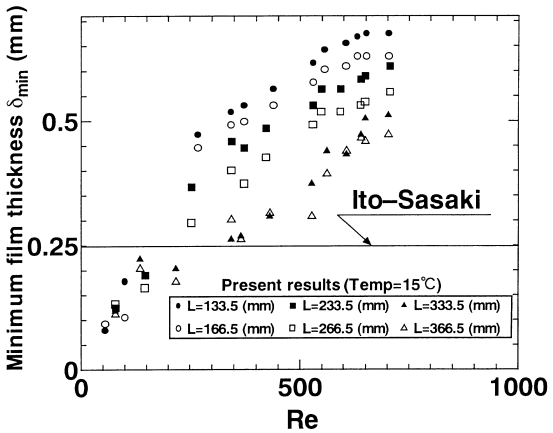

Fig. 17. Minimum film thickness.

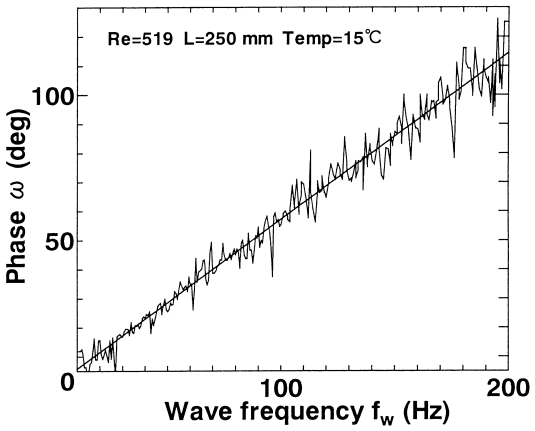

Fig. 19. Wave frequency and the phase lag.

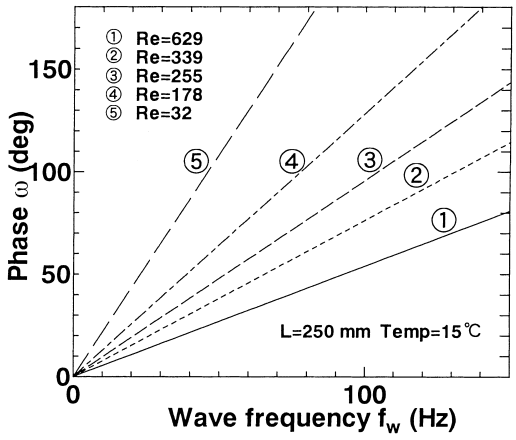

Fig. 20. Effect of flow rate on wave frequency and phase lag.

LFDs. A typical result of the phase lag of waves between the LFDs is shown in Fig. 19. A simple linear relationship between the wave velocity and wave frequency, as well as phase lag, can be given by Eq. (6), under the assumption that the wave velocity is independent of the frequency. The straight line in the Fig. 19, which expresses a linear relationship, is derived by the least squares method. Fig. 20 shows the effect of liquid flow rate on the phase lag. As shown in the figure, the slope is gentler, indicating that the wave velocity increases as the flow rate or the Reynolds number increases.

Fig. 21 shows the relationship between the wave velocity calculated from Eq. (6) and the Reynolds number. The broken line and solid line represent Ito–Sasaki's empirical equation (21) [15], and a theoretical equation calculated from Nusselt's law (22) [10], respectively.

$$C_W = 5.91 \times 10^{-2} Re^{0.45} \tag{21}$$

$$C_W = \frac{3}{2}\left[\frac{g\nu}{3}\right]^{1/3} Re^{2/3} \tag{22}$$

The present data with $L = 250$ mm, expressed by solid circles, agree well with Nusselt's theoretical equation, indicating the flow to be laminar even at a high flow rate, as do the present results for average film thickness.

Fig. 22 shows the calculations of dimensionless wave velocity, $\alpha\,(= C_W/U_0)$ defined by average liquid velocity $U_0\,(= \Gamma/\bar{\delta})$. In the figure,$\alpha = 3$ obtained Kapita' s linear theory [16] and $\alpha = 2.4$ obtained by Levich–Bushmanov's non-linear theory [17] are plotted. The results of $\alpha = 1.2$–1.4 in the present experiments are much smaller than those obtained from the theories with the sole exception of $\alpha = 2.16$ in the case of $Re = 30$. An assumption of very low liquid flow rate used in the theories might cause the discrepancy between the results of the theories and the present experiments.

Recently, the relationship among wave velocity, maximum film thickness, and wave separation in an entry region have been studied experimentally by Nosoko et al. [18] in the range of $Re = 14 - 90$. They used a needle-contact technique to measure the maximum film thickness at a position of 100 mm from the film entrance, and used photographs taken with a synchronized stroboscope to measure wave separation and velocity. The following empirical equations were drawn from their study:

$$N_{\delta_{max}} = 0.49 K_F^{0.044} N_\lambda^{0.39} Re^{0.46} \tag{23}$$

$$N_{C_W} = 1.13 K_F^{0.02} N_\lambda^{0.31} Re^{0.37} \tag{24}$$

where $N_{\delta_{max}}$, N_{C_W}, N_λ, and K_F are the dimensionless

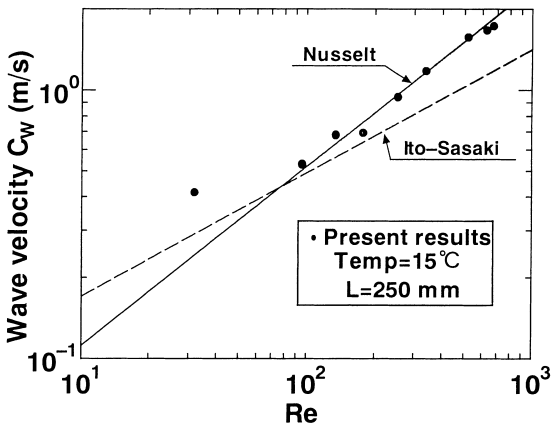

Fig. 21. Wave velocity.

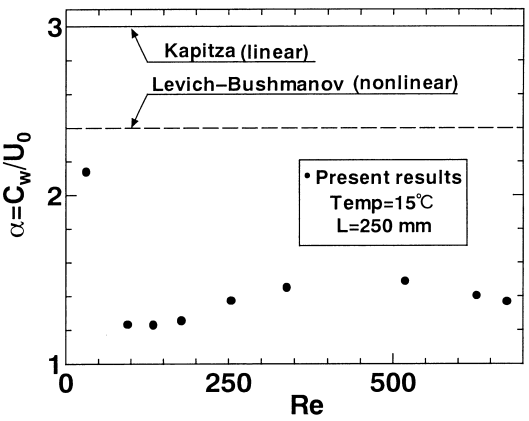

Fig. 22. Dimensionless wave velocity.

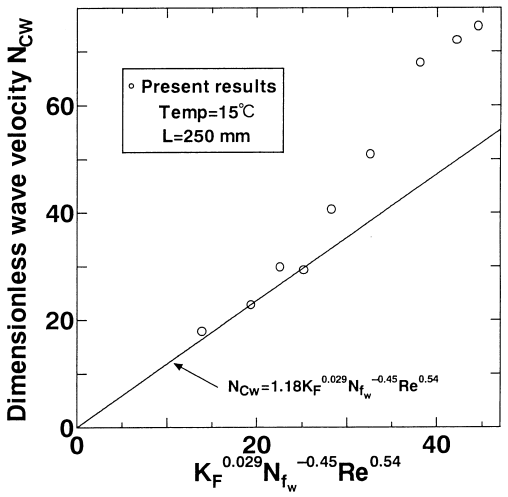

Fig. 23. Dimensionless wave velocity and Nosoko's correlation.

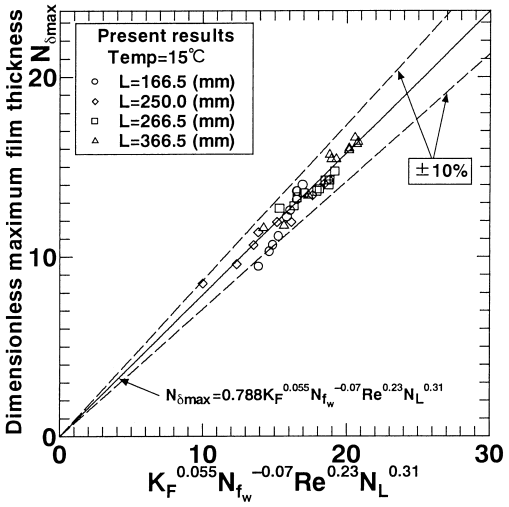

Fig. 25. Dimensionless maximum film thickness and the present equation.

maximum film thickness, wave velocity, wave separation, and physical properties group, respectively.

In the present study, wave frequency was measured with the LFD, which gives temporal information of the wave interface. To estimate the effect of wave frequency on wave velocity and maximum film thickness, the equations are modified with the dimensionless wave frequency N_{f_W} $(= N_{C_W}/N_\lambda)$ as follows:

$$N_{C_W} = 1.18K_F^{0.029}N_{f_W}^{-0.45}Re^{0.54} \quad (25)$$

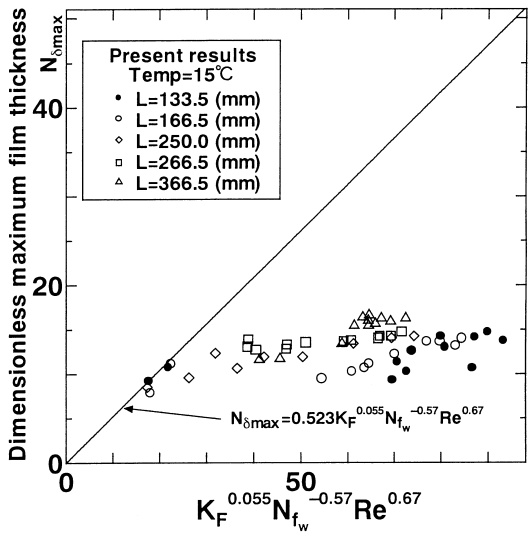

Fig. 24. Dimensionless maximum film thickness and Nosoko's equation.

$$N_{\delta_{max}} = 0.523K_F^{0.055}N_{f_W}^{-0.57}Re^{0.67} \quad (26)$$

The interfacial waves on film consist of waves differing in amplitude and frequency. Chu and Dukler classified the waves into three types: large waves, small waves, and base waves [19]. A large wave implies that a large fluctuation takes place about the average film thickness, $\bar{\delta}$, with minimum and maximum film thickness associated with the wave being alternate sides of $\bar{\delta}$. Figs. 23 and 24 show the relationships between the equations and the present results for large waves. Although the present data agree well with the equations in the low Reynolds number region, $Re < 100$, they do not agree well in the high Reynolds number region, $Re > 100$, and in the long entry region, $L > 250$ mm. A curve fit to collapse the data has been applied using the dimensionless entry length, N_L, and the least squares method. The present data are described within a $\pm 10\%$ deviation by the following equation as shown in Fig. 25.

$$N_{\delta_{max}} = 0.788K_{Fxs}^{0.055}N_{f_W}^{-0.07}Re^{0.23}N_L^{0.31} \quad (27)$$

5. Conclusion

This report presents an experimental study measuring waves on a film flowing down a vertical plate wall using a pair of laser focus displacement meters, LFDs. The purpose of the study was to clarify the effectiveness of the new method for obtaining detailed information on waves, including the minimum and maximum film thickness or wave heights, the average

film thickness, and the velocity and frequency of the waves, and to investigate the effect of length down from the film entrance on the phenomena. The results are summarized as follows.

It was possible to measure the liquid film flowing down a transparent plate wall using an LFD from the back of the plate. The error caused by the refraction of the laser beam passing through an acrylic plate and water was estimated by Eq. (4). Wave on the film flowing down a plate wall grew rapidly at low liquid flow rates or small Reynolds numbers. The reason for this was that the time required to reach the measurement position became a key factor in the growth of the wave. The present data for average film thickness and wave velocity agreed with Nusselt's theoretical equation in the short entry region, thus indicating the flow to be laminar even at a high flow rate. The results for maximum and average film thickness, as well as standard deviation of the film thickness, indicated that the wave behaviors were independent of the entry length in low Reynolds number conditions, with $Re < 250$. As a result of this study, an empirical equation (27) expressing the relationship between the frequency of large waves and flow rate, as well as the entry length, was formulated.

Acknowledgements

The authors would like to thank Mr. K. Kobayashi (Graduate School of Marine Engineering, Tokyo University of Mercantile Marine) for his help in conducting the experiments.

References

[1] S. Poltalski, A.J. Clegg, An experimental study of wave inception on falling liquid film, Chemical Engineering Science 27 (1972) 1257–1265.
[2] K. Mori, T. Matsumoto, H. Uematsu, Time-spatial interfacial structures and flow characteristics in falling liquid film, in: Proceedings of Third International Conference on Multiphase Flow, CD-Rom, 1998, #514.
[3] A. Elsäßer, W. Samenfink, J. Ebner, K. Dullenkopf, S. Wittig, Effect of variable liquid properties on the flow structure within, Proceedings of Ninth Intenational Symposium on Application of Laser Techniques to Fluid Mechanics 1 (3) (1998) 1–10.
[4] A.E. Dukler, O.P. Bergelin, Characteristics of flow in falling liquid film, Proceeding of Chemical Engineering Progress Symposium Series 48 (11) (1952) 557–563.
[5] G.F. Hewitt, N.S. Hall-Taylor, Annular Two-phase Flow, Pergamon Press, Oxford, 1970.
[6] M. Nasr-Esfahany, M. Kawaji, Turbulence structure under a typical shear induced wave at a liquid/gas interface, Proceedings of AIChE Symposium Series 310 (92) (1996) 203–210.
[7] A. Serizawa, T. Kamei, I. Kataoka, Z. Kawara, T. Ebisu, K. Torikoshi, Measurement of dynamic behavior of a liquid film flow with liquid droplets in a horizontal channel, Proceedings of Second International Conference on Multiphase Flow 2 (1995) 27–34.
[8] H. Takahama, S. Kato, Longitudinal flow characteristics of vertical falling liquid film without concurrent gas flow, International Journal of Multiphase Flow 6 (1980) 203–215.
[9] K. Mori, K. Sekoguchi, A. Yoshida, H. Tsujino, Chaotic characteristics in time-varying thickness of falling liquid film, Transaction of the Japan Society of Mechanical Engineers (in Japanese) 58 (550B) (1992) 1838–1845.
[10] W. Nusselt, Der Wärmeaustausch am Berieselungskühler, VDI-Z 67 (9) (1923) 206–216.
[11] Brauer, H., 1956. Strömung und Wärmeübergang bei Rieselfilmen. Vdi-Forschungshelt, 22(45).
[12] T. Aragaki, S. Toyama, H.M. Salah, K. Murase, M. Suzuki, Transitional zone in falling liquid film, Journal of Chemical Engineering Society (in Japanese) 13 (3) (1987) 373–375.
[13] W.H. Henstock, T.J. Hanratty, Gas absorption by a liquid layer flowing on the wall of a pipe, AIChE Journal 25 (1976) 122–132.
[14] K.J. Chu, A.E. Dukler, Statistical characteristics of thin, wavy films, AIChE Journal 20 (4) (1974) 695–706.
[15] A. Ito, M. Sasaki, Breakdown and formation of a liquid film flowing down an inclined plane, Transaction of the Japan Society of Mechanical Engineers 52 (475B) (1986) 1261–1265.
[16] Kapitza, P.L., Wave flow of thin layers of viscous, Collected Papers of P.L. Kapitza, 2, 1964, pp. 662–713.
[17] V.G. Levich, in: Physiochemical Hydrodynamics, Prentice-Hall, Englewood Cliffs, NJ, 1962, pp. 683–693.
[18] T. Nosoko, P.N. Yosimura, T. Nagata, K. Oyakawa, Characteristics of two-dimensional waves on a falling liquid film, Chemical Engineering Science 51 (5) (1996) 725–732.
[19] K.J. Chu, A.E. Dukler, Statistical characteristics of thin, wavy films, AIChE Journal 20 (4) (1974) 695–706.